© 1967 IEEE. Personal use of this material is permitted. However, permission to reprint/republish this material for advertising or promotional purposes or for creating new collective works for resale or redistribution to servers or lists, or to reuse any copyrighted component of this work in other works must be obtained from the IEEE.

STUDIES OF BEAM BEHAVIOR IN THE ENERGY REGION OF 50-400 MeV WITH THE BROOKHAVEN ALTERNATING GRADIENT SYNCHROTRON.*

A. van Steenbergen
Brookhaven National Laboratory
Upton, N.Y.

Summary. The "fast kicker" of the Brookhaven National Laboratory's AGS, normally used for orbit perturbation at high energy as part of the fast ejected beam system is used to eject the circulating proton beam in the energy region of 50-400 MeV. Beam behavior in the early part of the acceleration cycle is studied by measuring the ejected beam vertical phase space emittance and density distribution. Effective phase space dilution and beam intensity dependent effects have been observed. The observed distributions are consistent with a four or six dimensional gaussian distribution.

Introduction

Related to the desire of obtaining higher proton beam intensities in the AGS a considerable amount of effort has been devoted in recent years to the study of particle losses during the acceleration cycle. Knowledge of the beam emittance and its transverse phase space distribution during the acceleration cycle might help to provide information related to loss behavior, coherent oscillation behavior, and high beam density phenomena. So far, this technique has not been used to any extent as a beam diagnostic tool because of difficulties in measuring the beam emittance and its density distribution in the synchrotron ring.

For relatively low particle energies, the techniques for emittance measurement are well known by now.[1] Trying to apply these techniques to the measurement of the beam emittance in the synchrotron requires first of all an external beam channel and secondly modifications of these techniques, because of the high value of the kinetic energy of the particles involved.

Since a full aperture fast kicker[2] unit was available in the AGS, normally used for the high energy fast ejected proton beam, it was a simple matter to install an external beam channel immediately following the fast kicker unit. Beam emittance measurements were done in this external beam channel by operating the fast kicker unit at various times following beam injection into the synchrotron.

Experimental Arrangement

The general layout is shown in Fig. 1. To accommodate now a modified two slit emittance measurement technique, a horizontal slit is placed two magnets "downstream" in the deflected channel from the fast kicker unit. One magnet length (approximately 3.5 meters) downstream again, also in the deflected channel, a special wire target is located at the end of the external beam channel. Both the horizontal slit and the horizontal wire target are movable in the vertical direction, thereby providing for the measurement of the vertical transverse phase space projection.

The first slit is of "Heavy Met" (90% Tu) material with a thickness of 0.5 in. This thickness is about equal to the range value for protons of around 100 MeV kinetic energy. This corresponds then, for protons of 400 MeV to a $\Delta E/E$ value of around 25%. This is more than sufficient to discriminate the direct transmitted beam sample from the scattered background. The effect of slit scattering has been considered[3,4] and, with respect to the angular distribution of the direct beam sample at the location of L13, was found to be completely negligible.

To resolve the angular distribution of the beam sample, a thin wire target was chosen as a detector rather than the usual slit-Faraday cup approach. This, again because of the high kinetic energy of the particle beams involved.

Considerable effort was devoted in comparing the results of typical beam scans with the wire targets, with the results of Na^{24} activity counting following aluminum foil exposures in the same beam sample. Early results with simple (biased) targets indicated distribution half maximum width errors of up to plus 30%. The results with the present target agreed to within 5% with the results obtained with the aluminum foil exposure technique. This target consists now of a wire, 0.030 in. in diameter covered with the thinnest possible glass capillary, which in turn is painted with a conductive coat. This target is located in air in close proximity to the end of the external beam channel. The channel is kept under vacuum and is terminated with an aluminized Mylar window. Isolated from this is a thin (0.010 in.) copper stopper, which is directly connected to the outside conductor of a coaxial cable, which also is in turn connected to the outside conductor of the target.

The exact value of $\int Bdl$ of the magnetic structure of the fast kicker unit is not known and, therefore, the beam momentum ($\beta\gamma$ value), needed for emittance normalization, must be determined otherwise. This is done by measuring the frequency of the low level rf system, which is locked-in with the orbital frequency of the circulating protons, as a function of time. This together with an exact knowledge of the effective circumference of the proton orbits in the AGS yields β and consequently the proton

*Work done under the auspices of the U.S. Atomic Energy Commission.

momentum value.

It is desirable to relate the measured beam emittances in the external beam channel to the beam emittances in the synchrotron. For this purpose, and also for the purpose of the physical development of the external beam channel, maximum beam phase space ellipses in the synchrotron at locations of interest and in the external beam channel were calculated. This was done by A.R. Watts, using the computer program "BEAM". These results indicate that at the location of the vertical emittance measurement, the vertical emittance orientation is essentially identical with that in the synchrotron at the corresponding L12 location.

Phase Space Measurements

The phase space projection of the external proton beam is systematically and sequentially sampled by the scanning motion of the target and the beam sampling slit. This is done in a step wise fashion and during every machine pulse a sub-density value is measured by means of the total charge collected on the target. This is channeled to an integrating preamplifier which drives the long cable to the Main Control Room of the AGS. The following associated electronic circuits and data recording instrumentation are shown schematically also in Fig. 1. Since the sampling slit and target are integrating over the horizontal phase space components, in effect, the integrated partial density function D (y,y') is measured as a function of y and y'(y'= p_y/p_z), whereby D (y,y') = $\int\int\rho(x,x',y,y')\,dx,dx'$. The magnitude of this is superimposed on one of the channels of an XY recorder, which is linked in the indicated fashion directly to slit position and target position. A typical example of an emittance measurement with density distribution is indicated in Fig. 2. Here, various levels equi-density contours are indicated showing the density distribution in the two dimensional phase space projection. In addition, after a complete sequence of target motion, but before the first slit is moved to the next position, the value of the $[\int D(y,y')dy']_{y=y_i}$ is taken automatically. These values are then plotted as a function of vertical position on the same graph and are also indicated in Fig. 2, indicating the density distribution in real space of the proton beam. A transformation of these last results may be obtained directly by scanning with the target with the first slit removed from the beam. A more direct way of obtaining the real space beam distribution at the L12 location may be done by scanning with the slit and locating at L13 a large diameter target constructed similarly to the "wire" target, as indicated in the foregoing. Examples of results obtained in either fashion are also given in Fig. 2.

The 10% equi-density contour, as shown on the emittance plot, is assumed to be the emittance value of the proton beam under consideration. Integration, to determine particle content within this contour, for various conditions and beam momenta, always yielded particle content within this contour of approximately 90% to within ± 5%. Results of phase space area measurement as discussed below always refer to this particular definition of beam emittance.

Emittance Behavior for High and Medium Intensity Beams

To investigate the behavior of the beam emittance during the early part of the acceleration cycle and its possible relationship to total beam intensity, the vertical beam emittance was measured as a function of time with optimum AGS performance. Under these conditions final accelerated beam intensity, during this period, was approximately $1.9\ 10^{12}$ pr/p. This was immediately followed by a similar experimental run during which the only change in conditions was the dilution of the injected beam transverse phase space by a factor of 2.

A lower injected beam intensity could be obtained by reducing the injected number of turns into the AGS, however, in this particular case the value of the horizontal phase space is expected to be different and because of expected coupling between horizontal and vertical motion, vertical results could be affected by this. Further, the linac vertical and horizontal beam emittance varies as a function of time in either of the transverse coordinate phase space projections. Typically, if the linac beam emittance is measured with a delayed 8 μsec gated detector as compared with the full pulse length measurement the overall emittance value of the long beam pulse might be as much as a factor of 1.5 larger than the value obtained when measuring with the 8 μsec "bite" from the total beam pulse. Also, the time dependence variation has been measured in this fashion.

The beam intensity behavior (N) as a function of time for the high intensity run is indicated in Fig. 3, together with (dN/dt). An example of the measured phase space for both intensities at a particular beam momentum is shown in Fig. 4a. The enlargement of the beam emittance related to beam intensity only is approximately 1.3; the average two dimensional density is higher by only approximately 20%, for the higher intensity case, at this time after injection, notwithstanding that the injection dilution factor was 2.

The emittance behavior as a function of time for high beam intensity and medium intensity has also been indicated in Fig. 3. Considering the high intensity behavior as a function of time, it is seen that immediately after injection the beam fills the apparently available vertical acceptance. During the first few msec after injection some shrinking of the vertical emittance takes place, followed immediately, however, by an anomalous behavior, where no shrinking of the absolute emittance area takes place and whereby the normalized phase space actually grows as a function of time. The reduction of the emittance after

about 7 msec seems related to a pronounced loss preceding this, as may be observed from $(dN/dt) = f(t)$.

The anomalous increase and decrease in the region of about 11 msec is not paired by a simultaneous beam loss. It is at present assumed to be a coherent growth and decay of the magnitude of the vertical phase space, possibly caused by the transition through the $\nu_x - 2\nu_y = -9$ coupling resonance, as will be further discussed below. Following the slow decrease of the normalized phase space as a function of time, which seems paired with a small "bump" loss and some continuous particle loss, at 20 msec a pronounced growth of the normalized phase space takes place, followed by a significantly lower $\beta\gamma A_{2,v}$ value. No appreciable loss takes place in this time domain and no satisfactory explanation for this decrease is available. It is known that for less ideal AGS conditions normally a pronounced loss occurs at about this time, associated with the transition through the $\nu_x = 8\frac{1}{2}$ stop band. After about 25 msec, $\beta\gamma A_{2,v}$ approaches the invariant value, with some indication of a coherent growth and decay at around 32 msec. For reasons to be indicated below, this is again speculated to be connected with the transition through the coupling resonance condition $\nu_x - 2\nu_y = -9$.

Observing the medium intensity vertical emittance behavior as a function of time, it is observed that the beam does not fill the available acceptance, which on the previous run was found to be $A_{2,v} = 11.6$ cm-mrad. Following some initial shrinking of the normalized phase space area, again a pronounced growth occurs around 5 msec after injection. Since this has not been observed at lower beam intensities, with single turn injection, it is thought to be an intensity dependent blow up of the effective phase space. The invariant $(\beta\gamma A_{2,v}) = \text{constant}$ condition is reached about 20 msec after injection in this particular case.

The normalized vertical emittance as a function of momentum for these runs is indicated in Fig. 5. Here it is possible to indicate the apparent maximum acceptance by a straight line. It is in general instructive to note that the maximum available vertical phase space acceptance is almost a factor of 2 smaller than the calculated value when taking into account the minimum AGS aperture at a vertical β_{max} value, notwithstanding that the performance of the AGS during these studies was optimum.

Some of the facets of the behavior of the vertical emittance as a function of time becomes more difficult to explain when considering $(\delta_2)_{av} = \left(\frac{N}{\beta\gamma A_{2,v}}\right)_{av.}$ the normalized vertical two dimensional phase space density, as a function of time. This is also indicated in Fig. 5 for the normal and "diluted" case. Assuming no coupling, $(\delta_2)_{av.}$ can only increase when particle loss is relatively small and the phase space shrinking is pronounced by scraping of the low density regions of the periphery of the phase space distribution. Even using these simple assumptions it is hard to explain, with the present limited amount of data, the particular features of both the high intensity and low intensity $(\delta_2)_{av.} = f(t)$ behavior.

It is obvious that knowledge of the vertical phase emittance as a function of time is not sufficient and that coupling between vertical and horizontal motion must be taken into account. Instrumentation is presently being assembled for measurement also of the horizontal emittance together with the vertical emittance.

Some characteristics of the high intensity $(\beta\gamma A_{2,v}) = f(t)$ behavior can possibly be explained when considering the ν_x, ν_y values between injection and 40 msec after injection. Coherent ν values near injection for the AGS are indicated on a ν_y versus ν_x diagram, Fig. 6. These ν values were measured by E. Raka and D. Robertson, as indicated. Actually, the ν_x, ν_y value at injection for $N_f = 1.9\ 10^{12}$ pr/p has been extrapolated from the Robertson results by considering the theoretical coherent $\Delta\nu_y$ as a function of N. The intensity dependent incoherent ν_y depression is, according to the Laslett[5] theory, estimated to be a factor of 3 larger than the coherent $\Delta\nu$ value and this, together, with the inverse proportionality of $\Delta\nu_y$ with $\beta^2\gamma^3$ leads to a speculated ν_x, ν_y trajectory, for $N_{fin} \cong 2\ 10^{12}$ pr/p, for the AGS. This behavior of the working point is enforced by the observed effect of the "skew quadrupole" resonance line, $\nu_x + \nu_y = 17$*. Following this trajectory, the characteristics of the emittance as a function of time become somewhat more plausible and the suggestion of the traversal twice of the coupling resonance, $\nu_x - 2\nu_y = -9$, for the high intensity case, seems reasonable.

Effective Phase Space Dilution

Since at all times during these studies the linac emittance is measured simultaneously, effective dilution during the injection process can be evaluated. The linac emittance is also indicated in Figs. 3 and 5. The "zero" time value on these graphs is actually 80 μsec after the start of the injection process. The effective dilution values are summarized in Table I. The results indicate that a pronounced increase of the (effective) vertical phase space takes place at "injection", apparently related to total charge injected. Further, for the beam intensities under consideration, even with single turn injection, the effective overall increase (after 40 msec) of

*A. Maschke, private communication.

the normalized phase space area is appreciable and larger than heretofore estimated.

Single Turn versus Multiturn Injection

Some phase space measurements have been done with single turn injection into the synchrotron as opposed to multiturn injection. Some of these results are also indicated in Fig. 5 and data related to $A_{2,v}$ measurements at 80 μsec, for various number of injected turns, is indicated in Fig. 4b. The total injected charge varied in the latter case from $\cong 1\ 10^{12}$ to $8\ 10^{12}$ protons. Again, the "blow up" of the vertical emittance is such, that with more than four turns injection, the total synchrotron vertical phase space is filled immediately. Further studies are obviously needed to understand better this apparent intensity dependent behavior during the injection stacking process.

Phase Space Density Distribution

Some insight regarding the real particle density distribution in either the four or six dimensional phase space may be obtained by an analysis of the two dimensional distribution D(y,y') or the real space density distribution d(y), both of which have been measured in this work. Attempts have been made in the literature[6,7] to proceed from an assumed real space charge distribution, via analytical treatment, to a knowledge of the phase space distribution. An alternative way is to assume some simple, practically possible, distributions in either the four or six dimensional phase space. By integration, D(y,y') and d(y) are obtained and by comparing these calculated distributions against the experimentally obtained D(y,y') and d(y) functions, some conclusions may be drawn with regard to the phase space distribution.

In the following several phase space distributions have been considered. Since a beam "waist" exists at the AGS straight section location L5 in both the horizontal and vertical phase space projection the assumed distributions refer to this azimuthal location. Following this, the results are transformed to observation location (L12) in the external beam channel. The total analysis is lengthy and, therefore, only the results and conclusions will be given.

a) Kapchinskij-Vladimirskij distribution[8], four dimensional phase space. $\rho(x,x'y,y') = \rho_o\delta(F-F_o)$; this represents a uniform particle distribution on a four dimensional surface and results in $D(y,y') = \pi\rho_o$ and

$$d(y) = \frac{2\pi n_o F_o}{\delta_y}^{1/2}\left[1 - \left(\frac{y}{F_o^{1/2}\delta_y}\right)^2\right]^{1/2}$$

b) Homogeneous distribution, in four dimensional phase space, i.e.

$$\rho = \rho_o \text{ within } \left(\frac{x}{a}\right)^2 + \left(\frac{x'}{b}\right)^2 + \left(\frac{y}{c}\right)^2 + \left(\frac{y'}{d}\right)^2 = 1,$$

(L15 location)

$\rho = o$ otherwise. Integration yields,

$$D(y,y') = C_{z,z'}\,\pi\rho_o\,ab\left(1 - \frac{y^2}{c^2} - \frac{y'^2}{d^2}\right) \text{ and}$$

$$d(y) = \frac{4}{3}\,C_{zz'}\,\rho_o\pi\,abd\left[1 - \left(\frac{y}{c}\right)^2\right]^{3/2}$$

Transformation of D(y,y') to L12 and integration results in,

$$D(y,y') = C_{zz'}\,\pi\rho_o\,ab\,(1-A^2y^2-B^2y'^2-Cyy')$$

and

$$d(y) = \frac{4\pi abC_{zz'}\rho_o}{3B^3}\left[1 - \left(\frac{y}{c_{tr}}\right)^2\right]^{3/2} \text{ with}$$

A, B and C constants, related to the elements of the transfer matrix M(L5, L12) and $c_{tr} = f(A,B,C)$.

c) Homogeneous distribution, six dimensional phase space, i.e.

$$\rho = \rho_o \text{ within } \left(\frac{x}{a}\right)^2 + \left(\frac{x'}{b}\right)^2 + \left(\frac{y}{c}\right)^2 + \left(\frac{y'}{d}\right)^2 + \left(\frac{z}{e}\right)^2 + \left(\frac{z'}{f}\right)^2 = 1$$

$\rho = o$ otherwise. This distribution is somewhat unrealistically representing the longitudinal motion; even if the z,z' plane projection boundary would be elliptical, it is not expected to produce a "stationary waist" at L5. The resultant transformed D(y,y') and d(y) functions are

$$D(y,y') = \frac{\pi^2}{2}\,\rho_o\,abef\,(1-A^2y^2-B^2y'^2-Cyy')^2$$

and

$$d(y) = \frac{\pi^2}{2B^5}\,\rho_o\,abef\left[1 - \left(\frac{y}{c_{tr}}\right)^2\right]^{5/2}$$

d) Gaussian distribution, six dimensional phase space, i.e.

$$\rho = \rho_o\, e^{-\left[\left(\frac{x}{a}\right)^2 + \left(\frac{x'}{b}\right)^2 + \left(\frac{y}{c}\right)^2 + \left(\frac{y'}{d}\right)^2\right]} \times e^{-\left[\left(\frac{z}{e}\right)^2 + \frac{zz'}{f^2} + \left(\frac{z'}{g}\right)^2\right]}$$

From this, it follows that

$$\rho(x,x',y,y') = \rho_o \left[\frac{2efg\pi}{(e^2g^2 + 4f^2)^{1/2}}\right] \times$$

$$e^{-(\frac{x}{a})^2 + (\frac{x'}{b})^2 + (\frac{y}{c})^2 + (\frac{y'}{d})^2} \qquad (*)$$

The partial phase space projections consistent with this distribution are[1],

$$(\frac{x}{a})^2 + (\frac{x'}{b})^2 = 1$$

and simultaneously

$$(\frac{y}{c})^2 + (\frac{y'}{d})^2 = 1 \quad (\rho \leq 0.14\ \rho_o);$$

i.e. elliptical projections and a "waist" in either the xx' or yy' phase plane. It follows again, after integration and transformation, that

$$D(y,y') = \pi^2 \rho_o\ ab \left[\frac{2efg}{(e^2g^2 + 4f^2)^{1/2}}\right] \times$$

$$e^{-[A^2y^2 + B^2y'^2 - Cyy']} \quad \text{and}$$

$$d(y) = \pi^2 \rho_o\ ab \left[\frac{2efg}{(e^2g^2 + 4f^2)^{1/2}}\right] \times$$

$$\frac{\sqrt{\pi}}{B} e^{-(A^2 - \frac{C^2}{4B^2})y^2}$$

Comparison of the calculated functions with the experimental results has been made for d(y) and, so far only, for the special case of $D(y,y')_{y=o}$. Only for the gaussian distribution with $D(y,y')_{y=o} = D_o e^{-B^2y'^2}$ and $d(y) = d_o e^{-k^2y^2}$ did the theoretical distributions fit the experimental data.

*The case of the four dimensional gaussian distribution is essentially identical. The form in square brackets would be replaced by $C_{zz'}$.

Acknowledgments

In addition to the contribution by A.R. Watts, already mentioned in the foregoing, I want to acknowledge the enthusiastic support of A. McNerney, with the instrumentation problems and further the helpful assistance of R. Frankel and E. Gill, during the early part of the instrumentation assembly.

References

1. A. van Steenbergen, Proc. V Int. Conf. on High Energy Accel., Frascati, 311, Sept. 1965.
2. E.B. Forsyth, C. Lasky, BNL 910 (T373), 1965.
3. E.J. Burge, D.A. Smith, Rev. Sci. Instr. 33, 1371 (1962).
4. E.D. Courant, Rev. Sci. Instr. 22, 1003 (1951).
5. L.J. Laslett, Proc. 1963 Summer Study on Storage Rings, Accelerators and Experimentations at Super-High Energies, BNL 7534, 324.
6. T.R. Walsh, Plasma Physics, Journal of Nuclear-Energy, part C, 5, 17 (1963).
7. P.M. Lapostolle, CERN Rep., ISR-300, LIN/66-32, Oct. 1966.
8. I.M. Kapchinskij, V.V. Vladimirskij, Proc. Conf. on High Energy Accelerators and Instrumentation, CERN, 274 (1959).

Table I

$A_{2,v}$ measured at time	80 μsec	40 msec
$\frac{\beta\gamma A_{2,v}(10\text{ t.}, N_{in}= 7.7\ 10^{12})}{\beta\gamma A_{2,v}(\text{Linac, full pulse length})}$	2.5	2.0
$\frac{\beta\gamma A_{2,v}(10\text{ t.}, N_{in}= 3.8\ 10^{12})}{\beta\gamma A_{2,v}(\text{Linac, full pulse length})}$	1.9	1.5
$\frac{\beta\gamma A_{2,v}(1\text{ t.}, N_{in}= 1.2\ 10^{12})}{\beta\gamma A_{2,v}(\text{Linac, 8 μsec value})}$	(approx) 1.3	1.8

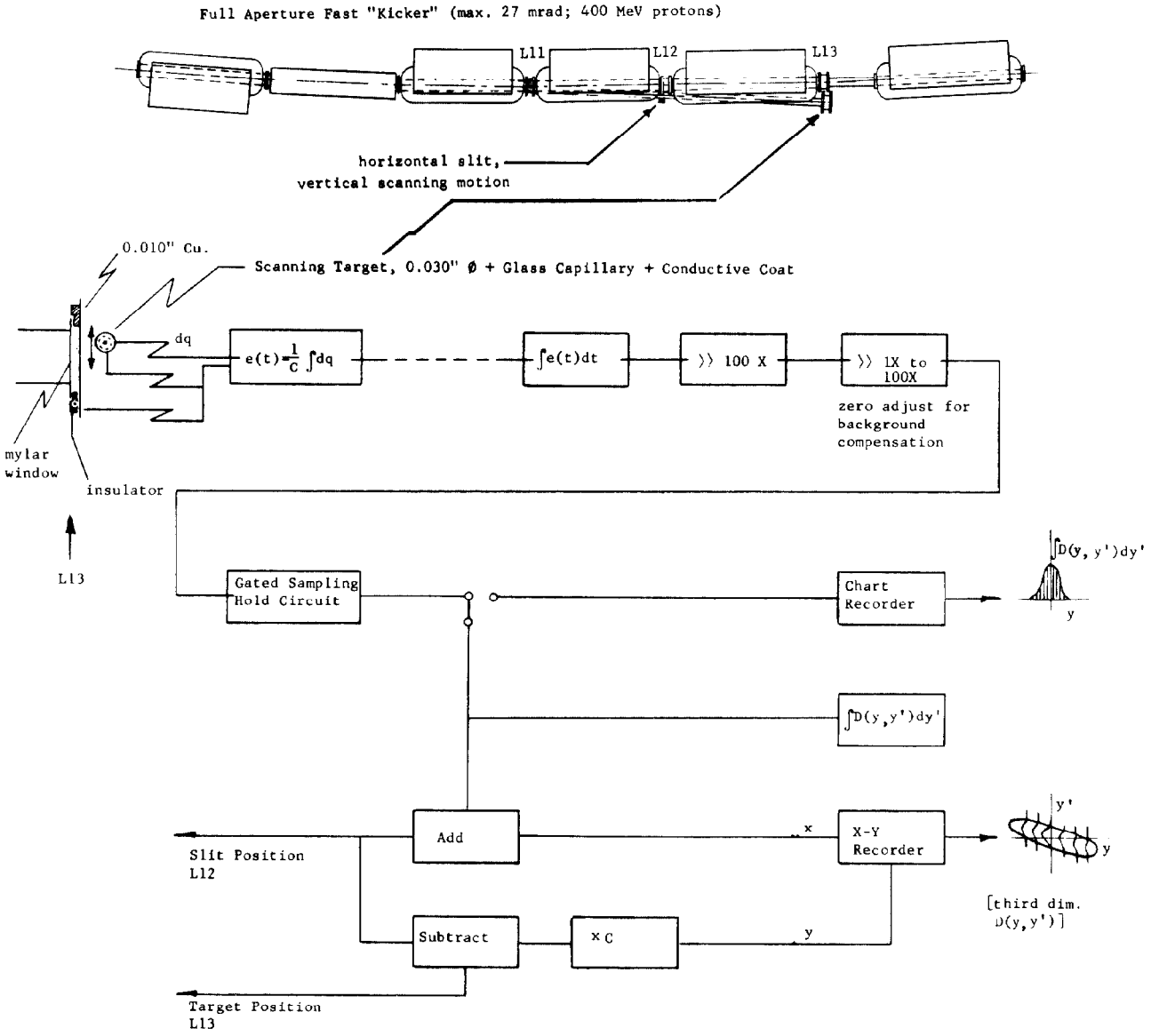

Fig. 1. Experimental Arrangement.

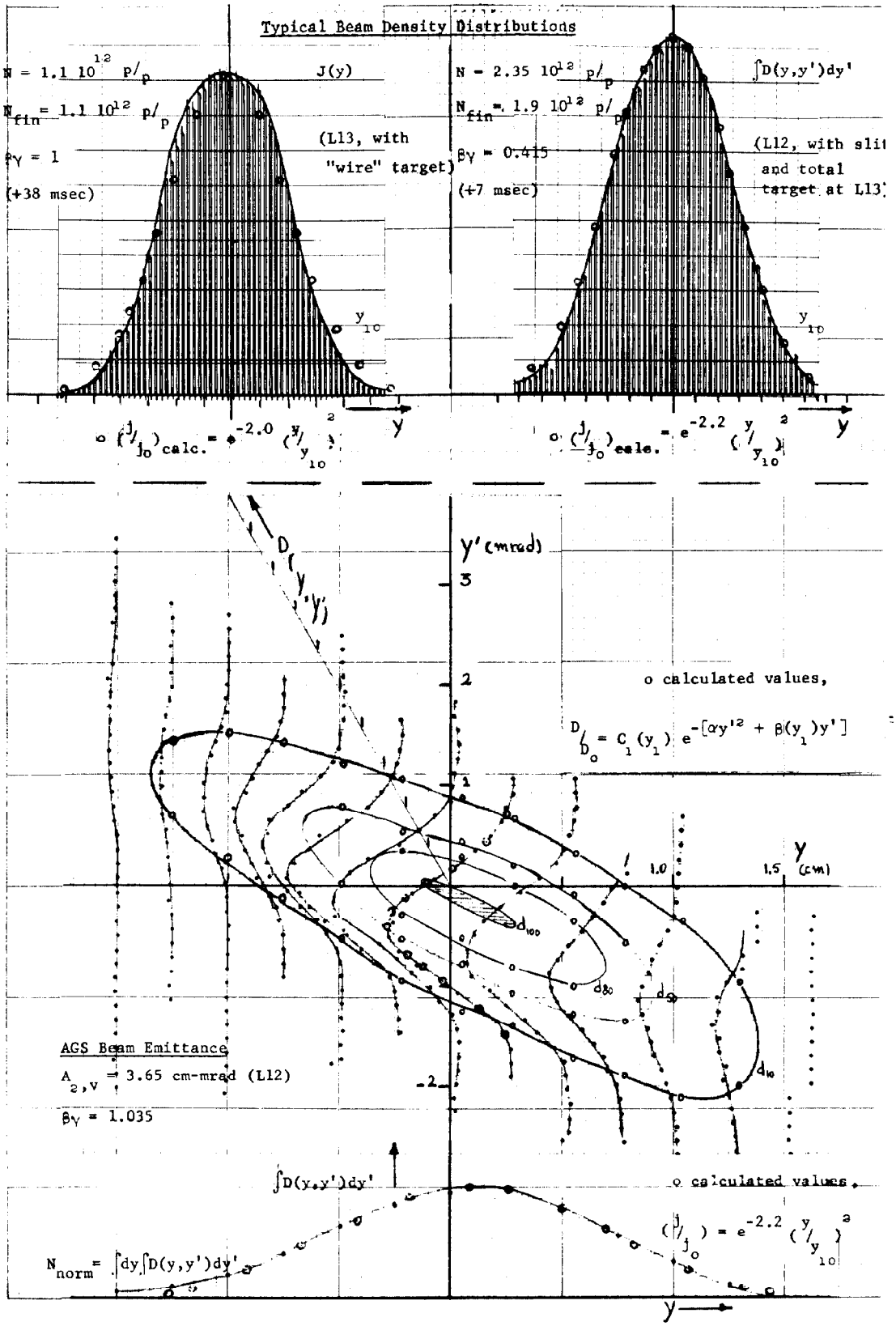

Fig. 2. Typical Beam Density Distributions.

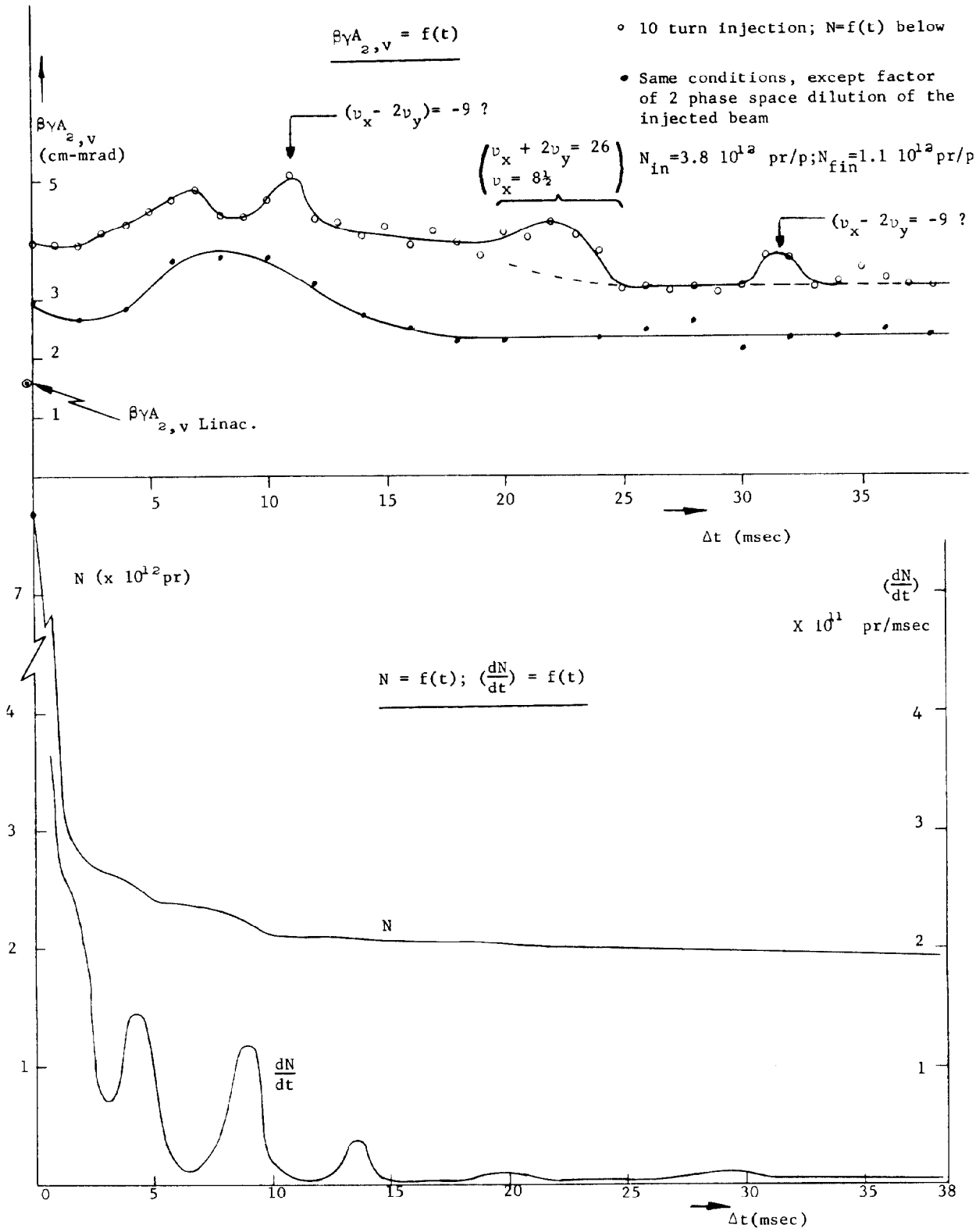

Fig. 3. $\beta\gamma A_{2,v} = f(t)$, $N = f(t)$; $\left(\frac{dN}{dt}\right) = f(t)$.

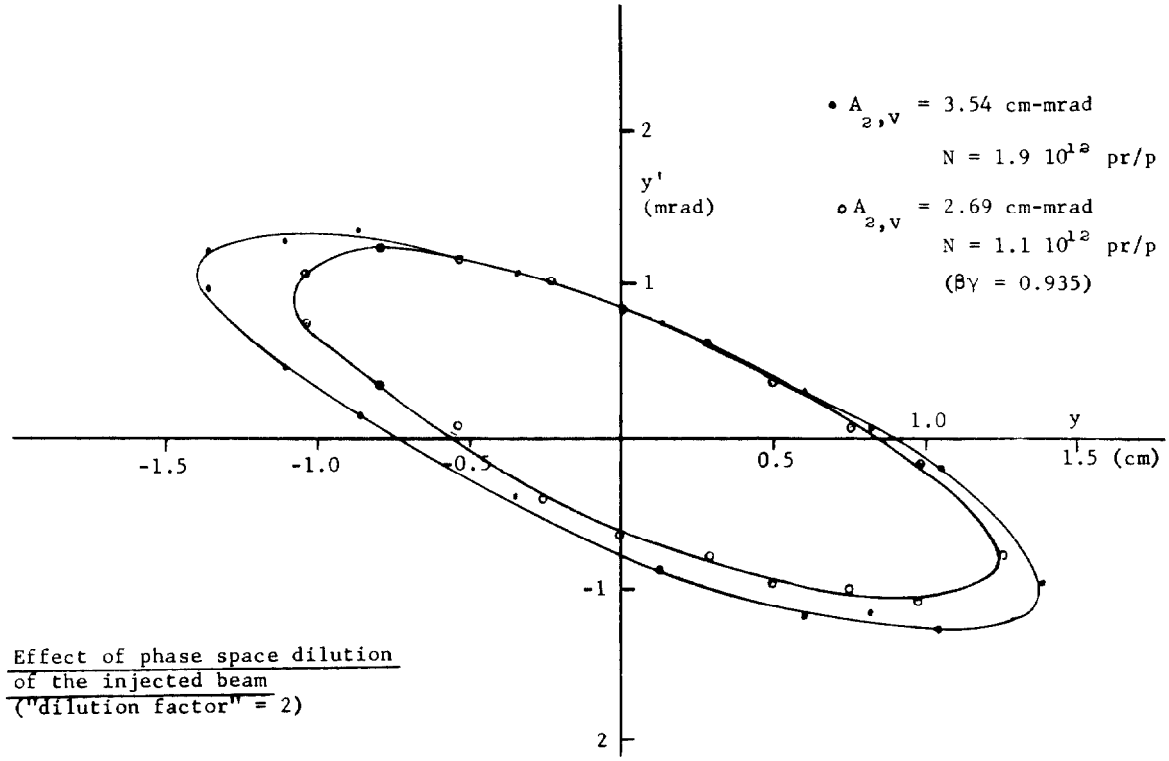

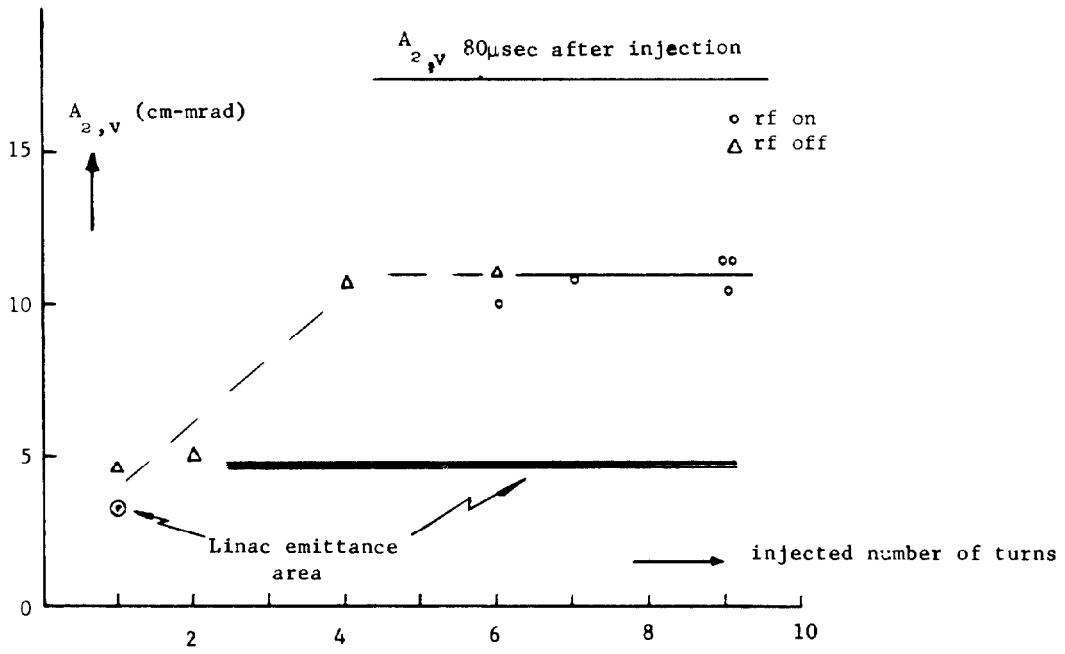

Fig. 4. Effect of Phase Space Dilution of the Injected Beam, $A_{2,v}$ 80 μ sec After Injection.

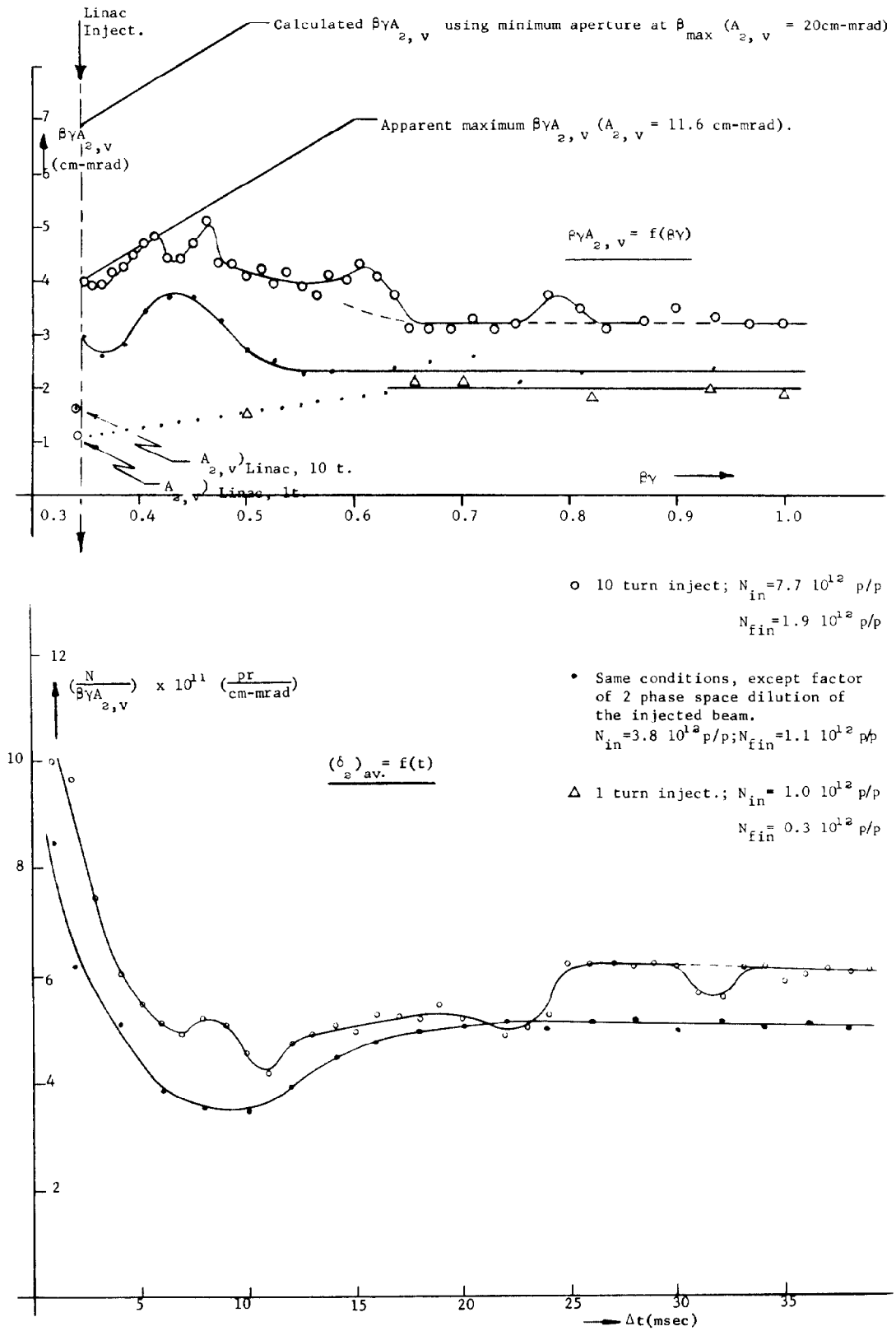

Fig. 5. $\beta\gamma A_{2,v} = f(\beta\gamma)$, $(\delta_2)_{av.} = f(t)$.

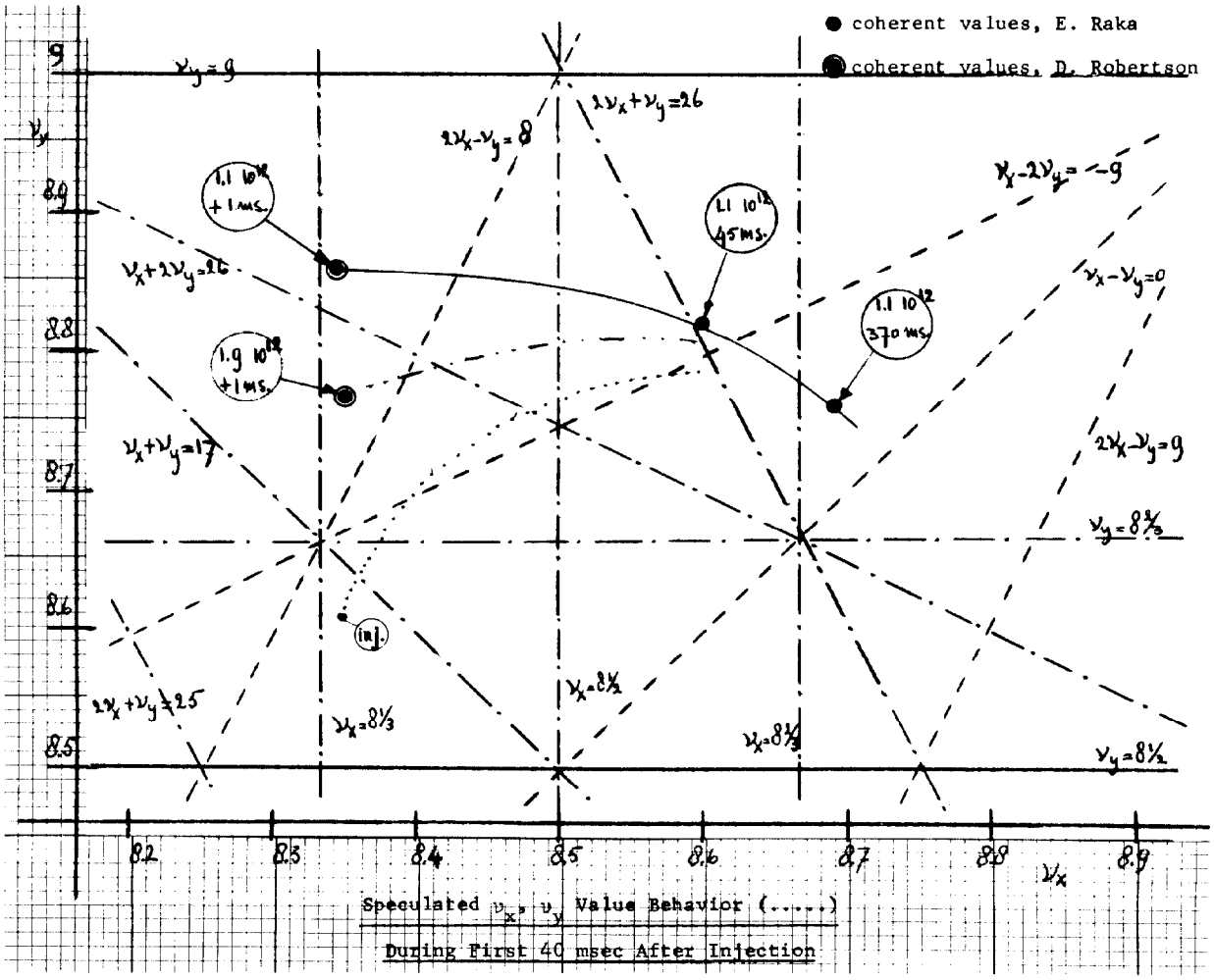

Fig. 6. Speculated ν_x, ν_y Value Behavior (. . . . .) During First 40 msec After Injection.